

High Resolution Spectroscopy of the X-ray Photoionized Wind in Cygnus X-3 with the Chandra High Energy Transmission Grating Spectrometer

Frits Paerels^{1,2}, Jean Cottam¹, Masao Sako¹, Duane A. Liedahl³, A.C. Brinkman², R.L.J. van der Meer², J.S. Kaastra², and P. Predehl⁴

ABSTRACT

We present a preliminary analysis of the 10 keV spectrum of the massive X-ray binary Cyg X-3, obtained with the High Energy Transmission Grating Spectrometer on the Chandra X-ray Observatory. The source reveals a richly detailed discrete emission spectrum, with clear signatures of photoionization-driven excitation. Among the spectroscopic novelties in the data are the first astrophysical detections of a number of He-like 'triplets' (Si, S, Ar) with emission line ratios characteristic of photoionization equilibrium, fully resolved narrow radiative recombination continua of Mg, Si, and S, the presence of the H-like Fe Balmer series, and a clear detection of a 800 km s^{-1} large scale velocity field, as well as a 1500 km s^{-1} FWHM Doppler broadening in the source. We briefly touch on the implications of these findings for the structure of the Wolf-Rayet wind.

Subject headings: atomic processes – techniques: spectroscopic – stars: individual (Cygnus X-3) – X-rays: stars

1. Introduction

In a previous paper (Liedahl & Paerels 1996, 'LP 96') we presented an interpretation of the discrete spectrum of Cyg X-3 as observed with the Solid State Imaging Spectrometers on ASCA (cf. Kitamoto et al. 1994; Kawashima & Kitamoto 1996). We found clear spectroscopic evidence that the discrete emission is excited by recombination in a tenuous X-ray photoionized medium, presumably the stellar wind from the Wolf-Rayet companion star (van Kerkwijk et al. 1992). Specifically, the ASCA spectrum revealed a narrow radiative recombination continuum (RRC) from H-like S, unblended with any other transitions. On closer inspection, RRC features due to H-like Mg and Si were also found to be present in the data, although severely blended with emission

¹Columbia Astrophysics Laboratory, Columbia University, 538 W. 120th St., New York, NY 10027, USA

²SRON Laboratory for Space Research, Sorbonnelaan 2, 3584 CA Utrecht, the Netherlands

³Department of Physics, Lawrence Livermore National Laboratory, P.O. Box 808, L-41, Livermore, CA 94550, USA

⁴Max Planck Institut für Extraterrestrische Physik, Postfach 1503, D-85740 Garching, Germany

lines. These narrow continua are an unambiguous indicator of excitation by recombination in X-ray photoionized gas, and their relative narrowness is a direct consequence of the fact that a highly ionized photoionized plasma is generally much cooler than a collisionally ionized plasma of comparable mean ionization (LP 96, Liedahl 1999 and references therein).

With the high spectral resolution of the Chandra High Energy Transmission Grating Spectrometer, we now have the capability to fully resolve the discrete spectrum. Apart from offering a unique way to determine the structure of the wind of a massive star, study of the spectrum may yield other significant benefits. Cyg X-3 shows a bright, purely photoionization driven spectrum, and, as such, may provide a template for the study of the spectra of more complex accretion-driven sources, such as AGN. The analysis will also allow us to verify explicitly the predictions for the structure of X-ray photoionized nebulae derived from widely applied X-ray photoionization codes.

2. Data Reduction

A description of the High Energy Transmission Grating Spectrometer (HETGS) may be found in Markert et al. (1994). Cyg X-3 was observed on October 20, 1999, for a total of 14.6 ksec exposure time, starting at 01:11:38 UT. The observation covered approximate binary phases

0:31 to +0:53, which means that about half of the exposure in our observation occurs in the broad minimum in the lightcurve at orbital phase zero. A spect-corrected data from the standard CXC pipeline (processing date October 30, 1999) was post-processed using dedicated procedures written at Columbia. We used (ASCA-)grade 0,2,3,4 events, a spatial filter 30 ACIS pixels wide was applied to both the High Energy Grating (HEG) and Medium Energy Grating (MEG) spectra, and the resulting events were plotted in a dispersion (CCD pulse height diagram, in which the spectral orders are neatly separated.

A second filter was applied in this dispersion (pulse height diagram. The filter consisted of a narrow mask centered on each of the spectral orders separately. The mask size and shape were optimized interactively. The residual background in the extracted spectra is of order 0.5 counts/spectral bin of 0.005 Å or less. The current state of the calibration does not provide us with the effective area associated with our joint spatial/pulse height filters to better than 25% accuracy, hence we have chosen not to flux-calibrate the spectrum at this time. An additional correction to the flux in the chosen aperture due to the (energy dependent) scattering of photons by interstellar dust has not yet been determined either.

In the resulting order-separated count spectra, we located the zero order and we determined its centroid position to find the zero of the wavelength scale. We then converted pixel number to wavelength based on the geometry of the HETGS. In this procedure, we used ACIS/S chip positions that were determined after launch from an analysis of the dispersion angles in the HETGS spectrum of Capella (Huenemörder et al. 2000). This preliminary wavelength scale

appears to be accurate to approximately 2 mÅ. The spectral resolution was determined from a study of narrow, unblended emission lines in the spectrum of Capella. It is approximately constant across the entire HETGS band, and amounts to approximately 0.012 Å (0.023 Å) FWHM for the HEG (MEG) (Dewey 2000). The resolution in the Cyg X-3 spectrum can be checked self-consistently by analyzing the width of the zero order image. Unfortunately, the zero order image is affected by pileup. However, enough events arrive during the 41 ms CCD frame transfer, forming a streak in the image, that we can construct an unbiased 1D zero-order distribution from them. The width of this distribution is consistent with the widths of narrow lines in the spectrum of Capella, which indicates that the resolution in the Cyg X-3 spectrum is not affected by systematic effects (e.g., incorrect aspect solution, defocusing).

3. X-ray Photoionization in Cyg X-3

Figure 1 shows the HEG and MEG first order spectra; the higher order spectra are unfortunately very weak, and we will not discuss them here. We show the spectra as a function of wavelength, because this is the most natural unit for a dispersive spectrometer: the instruments have approximately constant wavelength resolution. The spectra have been smoothed with a 3-pixel boxcar average to bring out coherent features. We have indicated the positions of expected strong H α and H ϵ -like discrete features. A cursory examination of the spectrum strikingly confirms the photoionization-driven origin of the discrete emission.

We detect the spectra of the H-like species of all abundant elements from Mg through Fe. In Si and S, we detect well-resolved narrow radiative recombination continua. This is illustrated in Figure 2, which shows the 3.0-7.0 Å band on an enlarged scale. The Si X IV and S XVI continua are readily apparent. The width of these features is a direct measure of the electron temperature in the recombining plasma, and a simple eyeball fit to the shapes indicates $kT_e \approx 50$ eV, which is roughly in agreement with the result of model calculations for optically thin X-ray photoionized nebulae (Kallman & McCray 1982). A more detailed, fully quantitative analysis of the spectrum will be required to see whether we can also detect the expected temperature gradient in the source (more highly ionized zones are also expected to be hotter). In the Si X IV and S XVI spectra we estimate the ratio between the total photon flux in the RRC to that in Ly α to be about 0.8 and 0.7, respectively; here, we assume $kT_e = 50$ eV, and we have made an approximate correction for the differences in effective area at the various features. These measured ratios are in reasonable agreement with the expected ratio of $0.73 (kT_e = 20 \text{ eV})^{+0.17}$ (LP 96), which indicates that the H-like spectra are consistent with pure recombination in optically thin gas.

The positions of the lowest members of the Fe XXV I Balmer series are indicated in Figure 1 (the fine structure splitting of these transitions is appreciable in H-like Fe, as is evident from the plot). The relative brightness of the Balmer spectrum is yet another indication of recombination excitation. There is evidence for line emission at the position of H δ , and possibly at H γ and H ϵ ; the spectrum is unfortunately too heavily absorbed to permit a detection of H β (9.52; 9.74 Å).

Unfortunately, the long-wavelength member of the H γ 'doublet' ($\lambda = 717$ Å) almost precisely coincides with the expected position of Al X III Ly γ , which precludes a simple and neat direct detection of Al (the first detection of an odd-Z triple- element in non-solar X-ray astronomy). Any limit on the Al/Si abundance ratio thus becomes dependent on an understanding of the intensity of the Fe XXV I spectrum.

As for the He-like species, we detect the $n = 2 \rightarrow 1$ complexes, consisting of the forbidden ('f'), intercombination ('i'), and resonance ('r') transitions, in Si X III, S XV, Ar XV II, Ca X IX, and Fe XXV (as well as the corresponding RRC in Si, S, and possibly Ar). The line complexes appear resolved into blended resonance plus intercombination lines, and the forbidden line (see Figures 1 and 2), up to Ar XV II.

In an optically thin, low density, purely photoionization-driven plasma, one expects the intensity ratio $f=(r+i)^{-1}$ for the mid-Z elements, very different from the pattern in the more familiar collisional equilibrium case, where the resonance transition is relatively much brighter (e.g., Gabriel & Jordan 1969; Pradhan 1982; Liedahl 1999). We use the ratio $f=(r+i)^{-1}$ rather than the conventional $G=(i+f)=r$ and $R=f=i$, because the intercombination and resonance lines are unfortunately blended by significant Doppler broadening in the source (see Section 4). Theoretically, in a photoionized plasma $f=(r+i)^{-1}$ is approximately equal to 1.3, 1.0, 0.83, for Si X III, S XV, and Ar XV II, respectively, and depends only weakly on electron temperature (LP 96, Liedahl 2000). The measured ratios $f=(r+i)^{-1}$, derived by fitting three Gaussians with common wavelength offset and broadening at the expected positions of f, i, and r, are approximately 1.1, 0.8, and 1.1 with the HEG, for Si, S, and Ar, respectively; the corresponding ratios for the MEG are 1.3, 1.0, and 0.8. Since most of the lines contain at least 100 photons, the statistical error on the ratios is generally less than 15%. These measurements include a model for the Si X III RRC in the S XV triplet (assuming $kT_e = 50$ eV), and Mg X II Ly γ emission in the Si X III triplet.

The He-like line ratios are probably affected by systematic features in the efficiency of the spectrometer. The S XV triplet is superimposed on the Si X III RRC, the Si X III triplet straddles the Si K edge in the CCD efficiency, and the Ar XV II triplet straddles the Au M $_{IV}$ and Ir M $_I$ edges. Corrections for these effects will have to be carefully evaluated. Nevertheless, the raw ratios $f=(r+i)^{-1}$ for the Si and Ar triplets are already of the right magnitude for pure recombination. Our provisional conclusion is that the He-like spectra are, very roughly, consistent with pure recombination in optically thin gas.

Just as in a collisional plasma, the relative strengths of the forbidden and intercombination lines are sensitive to density (Liedahl 1999; Porquet & Dubau 2000), due to collisional transfer between the upper levels of f and i at high density. As mentioned above, there are some systematic uncertainties in the measured line ratios, and we defer a discussion of possible constraints on the density in the wind to a future paper.

The detection of fluorescent Fe emission is a surprise, because virtually no fluorescence was seen at the time of the ASCA observation (Kitamoto et al. 1994). The apparent centroid

wavelength of the fluorescent line is 1.939\AA (photon energy 6394 eV), with a formal error of less than 10^{-3}\AA (3 eV). The width of the line is 0.022\AA FWHM, with a formal uncertainty of less than 5%. This is wider than would be expected from the velocity broadening to be discussed in the next section, and may be an indication that a range of ionization stages contributes to the fluorescent emission. If we assume the same velocity broadening for the Fe K feature as for the high-ionization lines (which may not necessarily be correct if the low- and high-ionization lines originate in different parts of the stellar wind), we find that Fe K has an intrinsic width (expressed as the FWHM of a Gaussian distribution) of 0.018\AA (corresponding to $E = 60\text{ eV}$). The fine structure split between $K_{\alpha 1}$ and $K_{\alpha 2}$ contributes slightly to this width ($\approx 0.004\text{\AA}$), but the measured width covers the full range of K wavelengths for charge states between fully neutral and Ne-like (Deraux et al. 1995).

4. Bulk Velocity Fields

We find that all emission features are significantly broadened and redshifted. The lines and radiative recombination continua are resolved by both the HEG and the MEG. The line widths for H-like Mg, Si, S, Ar, Ca, and Fe Ly were measured by fitting a simple Gaussian profile. Other than the negligibly small fine structure split ($\approx 0.005\text{\AA}$), these lines are clean and unblended. The resulting widths do not seem to exhibit a strong dependence on phase. Assuming that the spectrometer profile is well represented by a Gaussian of width 0.012\AA (0.023\AA) FWHM for the HEG (MEG), we find that the broadening of the lines is roughly consistent with a Gaussian velocity distribution, of width $v \approx 1500\text{ km s}^{-1}$ FWHM. The scatter is too large to permit a meaningful test for any dependence of the velocity broadening on ionization parameter. Note that no such broadening was seen in the spectrum of Capella.

We also measured the radial velocities for the Ly lines, assuming the dispersion relation obtained from an analysis of the spectrum of Capella. Wavelengths were calculated from the level energies given by Johnson & Scott (1985); these should be accurate to a few parts in 10^6 . There is a clear systematic redshift to all the emission lines and RRCs, in both the positive and negative spectral orders and in both grating spectra. This is shown in Figure 3, where we have segregated dim and bright state data, but have averaged positive and negative spectral orders, and HEG and MEG spectral data. Also shown are the best fitting uniform velocity offsets. These fits were forced to yield zero wavelength shift at zero wavelength. The average redshift for the dim state is 800 km s^{-1} , and for the bright state is 750 km s^{-1} . We thus find a net redshift much smaller than the observed velocity spread, and essentially no dependence of the centroid velocity on the binary phase. We should point out that our preliminary analysis, based on fitting simple Gaussians, is admittedly crude, and may have biased the true nature of the velocity field somewhat. We also note, with caution, that Doppler shifts due to a single, uniform velocity do not appear to be a very good description of the data: the longest wavelength lines appear to be offset at a significantly larger than average radial velocity. A detailed analysis, taking into account the

actual lineshape, will be required to confirm or refute the possibility that these offsets represent the expected systematic correlation of average wind velocity and ionization parameter.

5. Discussion

The HETGS spectrum of Cyg X-3 has revealed a rich discrete spectrum, the properties of which are consistent with pure recombination excitation in cool, optically thin, low density X-ray photoionized gas in equilibrium. We fully resolve the narrow RRCs for the first time, and estimate an average electron temperature in the photoionized region of $kT_e \approx 50$ eV, consistent with global photoionization calculations.

We detect a net redshift in the emission lines of $v \approx 750 - 800$ km s⁻¹, essentially independent of binary phase, and a distribution in velocity with a FWHM of ≈ 1500 km s⁻¹. If the wind were photoionized throughout, we would expect to see roughly equal amounts of blue- and redshifted material, so evidently we are viewing an ionized region that is not symmetric with respect to the source of the wind, as expected if only the part of the wind in the vicinity of the X-ray continuum source is ionized. However, in the simplest wind models, one would then expect to see a strong dependence of the centroid velocity on binary phase, alternating between red- and blueshifts, and this is decidedly not the case in our data. The implications of this finding for the flow pattern and distribution of material in the wind will be explored in a future paper.

Finally, the Fe K fluorescent feature, which probes a more neutral phase of the wind, has never been seen before in Cyg X-3. Unfortunately, the exact range of ionization can not be separated uniquely from systematic Doppler shifts through a measurement of the wavelengths of the K spectra, because the feature, while clearly broadened, is not separated into its component ionization stages. Still, the width of the feature (the net effect of the velocity field and the existence of a range of charge states) and its intensity will impose strong constraints on the global properties of the wind.

Acknowledgments.

We wish to express our gratitude to Dan Dewey and Marten van Kerkwijk, for discussions and a careful reading of the manuscript, and to the referee, Randall Smith, for a thorough review. JC acknowledges support from NASA under a GRSP fellowship. M S's contribution was supported by NASA under Long Term Space Astrophysics grant no. NAG 5-3541. FP was supported under NASA Contract no. NAS 5-31429. DL acknowledges support from NASA under Long Term Space Astrophysics Grant no. S-92654-F. Work at LLNL was performed under the auspices of the US Department of Energy, Contract no. W-7405-Eng-48.

REFERENCES

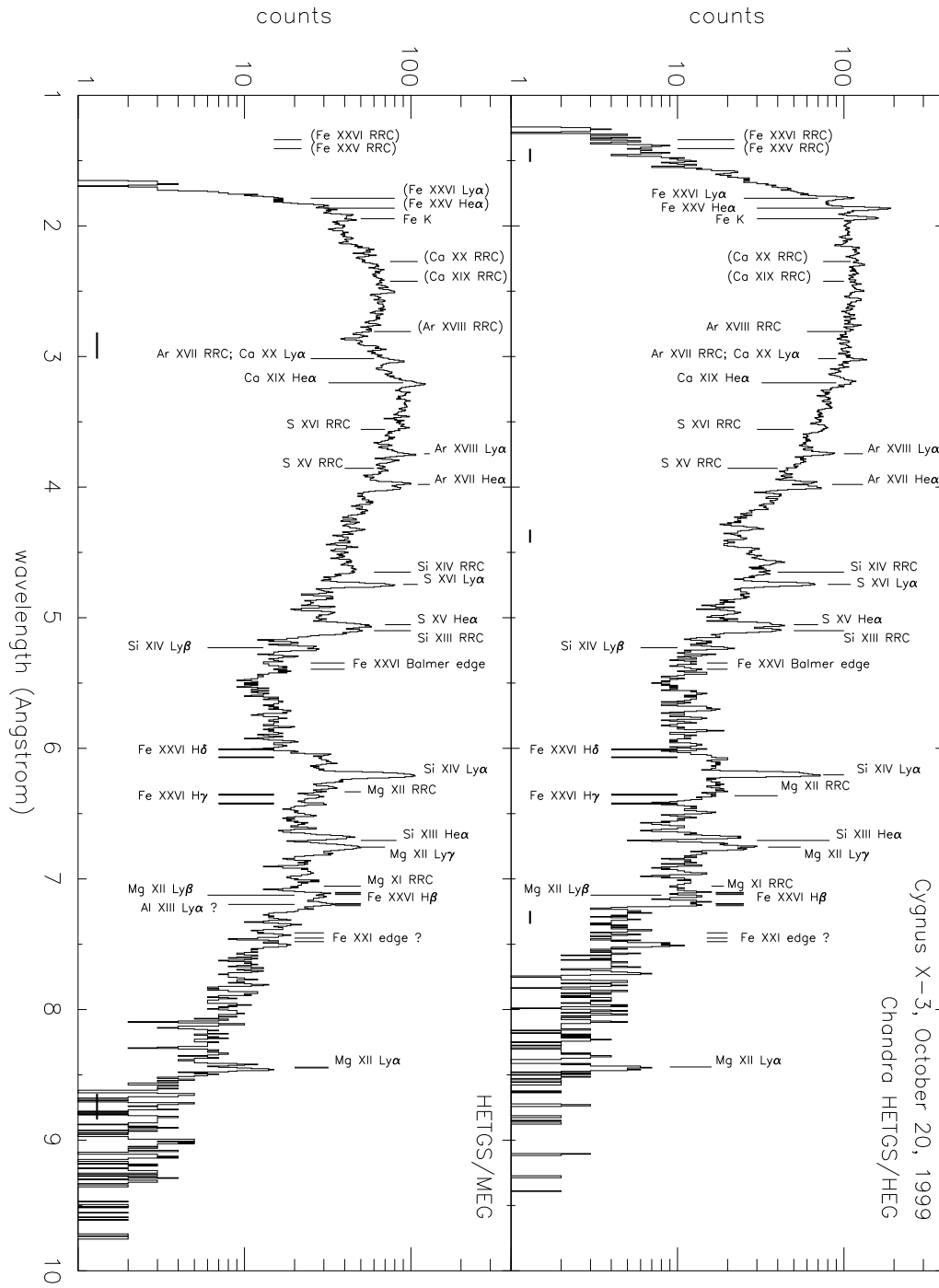
- Decaux, V., Beiersdorfer, P., Osterheld, A., Chen, M., & Kahn, S.M. 1995, *ApJ*, 443, 464.
- Dewey, D. 2000, *priv. comm.*
- Gabriel, A.H. & Jordan, C. 1969, *MNRAS*, 145, 241.
- Huenemörder, D., et al., *ApJ*, in preparation.
- Johnson, W.R., & Soderstrom, G. 1985, *Atom. Data Nucl. Data Tables*, 33, 405.
- Kallman, T.R., & McCray, R. 1982, *ApJS*, 50, 263.
- Kawashima, K., & Kitamoto, S. 1996, *PASJ*, 48, L113.
- Kitamoto, S., Kawashima, K., Negoro, H., Miyamoto, S., White, N.E., & Nagase, F. 1994, *PASJ*, 46, L105
- Liedahl, D.A., & Paerels, F. 1996, *ApJ*, 468, L33.
- Liedahl, D.A. 1999, in *X-ray Spectroscopy in Astrophysics*, Proceedings of the European Astrophysics Doctoral Network Tenth Summer School, J. van Paradijs & J.A.M. Bleeker (Eds.), p.189 (Berlin:Springer)
- Liedahl, D.A. 2000, in preparation.
- Markert, T.H., Canizares, C.R., Dewey, D., McGuirk, M., Pak, C., & Schattenburg, M.L. 1995, *Proc. SPIE*, 2280, 168.
- Porquet, D. & Dubau, J. 2000, *Rev. Mex. A.A.*, 99, 167.
- Pradhan, A. 1982, *ApJ*, 263, 477.
- van Kerkwijk, M.H., Charles, P.A., Geballe, T.R., King, D.L., Miley, G.K., Mohar, L.A., van den Heuvel, E.P.J., van der Klis, M., & van Paradijs, J. 1992, *Nature*, 355, 703.

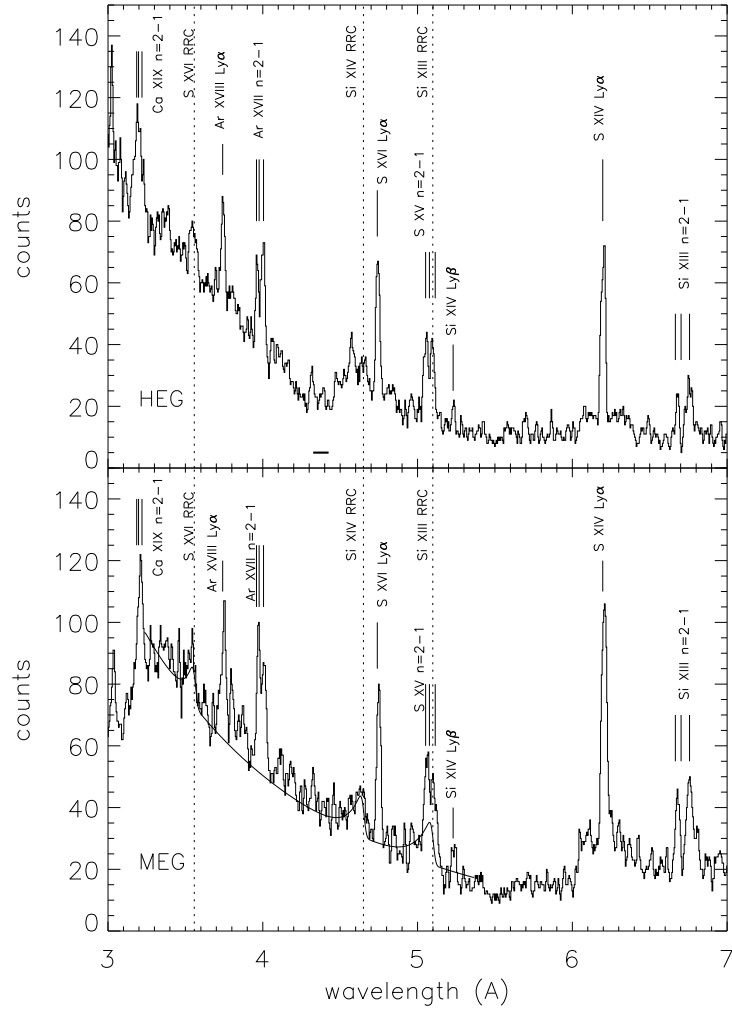
Figure Captions:

Fig.1 | The 1{10 Å spectrum of Cyg X-3 as observed with the HEG (upper panel), and the MEG (lower panel), binned in 0.005 Å bins. The positive and negative first orders have been added, and the spectra have been smoothed with a 3 pixel boxcar filter. Labels indicate the positions of various discrete spectral features. 'He' is the inelegant label for the resonance, intercombination, and forbidden lines in the He-like ions, plotted at the average wavelength for the complex. High-ionization features of interest that were not detected have been labeled in brackets. Horizontal bars indicate the nominal positions of the gaps between the ACIS chips; the dithering of the spacecraft will broaden the gaps and soften their edges.

Fig.2 | The 3.0{7.0 Å region of the spectrum enlarged; we show the raw count rates, binned by two 0.005 Å bins. The most important transitions have been labeled; dashed lines mark the expected positions of Si and S recombination edges. These markers have been redshifted by 800 km s⁻¹. The horizontal bar near 4.5 Å in the HEG spectrum marks the nominal position of the gap between chips S2 and S3 in ACIS. The solid line in the MEG spectrum is a crude empirical fit to the continuum, with SiXIII, SiXIV, and SXVI narrow radiative recombination continua added. The electron temperature was set to 50 eV, and the continua were convolved with a 1500 km s⁻¹ FWHM velocity field, to match the broadening observed in the emission lines.

Fig.3 | Measured wavelength shift for selected Ly features. Filled symbols refer to the 'dim' state data, open symbols to the 'bright' state data. The velocities as measured with the HEG and the MEG have been averaged; velocities in positive and negative spectral orders were averaged. Error bars indicate the size of the rms variation between these various measurements. In cases where only one or two velocities were measurable due to low signal-to-noise, we instead indicate the estimated statistical error on these measurements. The solid lines are the weighted least squares Doppler velocities for both the dim and the bright states.





{ 11 {

